AIAA 2002-0912
Improving Metallic Thermal Protection System Hypervelocity Impact Resistance Through Design of Experiments Approach

Carl C. Poteet
Max L.. Blosser
NASA Langley Research Center
Hampton, VA 23681-2199

40th Aerospace Sciences Meeting & Exhibit
14 - 17 January 2002
Reno, Nevada

AIAA 2002-0912

IMPROVING METALLIC THERMAL PROTECTION SYSTEM HYPERVELOCITY IMPACT RESISTANCE THROUGH DESIGN OF EXPERIMENTS APPROACH

Carl C. Poteet*, Max L. Blosser*
NASA Langley Research Center, Hampton, Virginia

Abstract

A design of experiments approach has been implemented using computational hypervelocity impact simulations to determine the most effective place to add mass to an existing metallic Thermal Protection System (TPS) to improve hypervelocity impact protection. Simulations were performed using axisymmetric models in CTH, a shock-physics code developed by Sandia National Laboratories, and validated by comparison with existing test data. The axisymmetric models were then used in a statistical sensitivity analysis to determine the influence of five design parameters on degree of hypervelocity particle dispersion. Several damage metrics were identified and evaluated. Damage metrics related to the extent of substructure damage were seen to produce misleading results, however damage metrics related to the degree of dispersion of the hypervelocity particle produced results that corresponded to physical intuition. Based on analysis of variance results it was concluded that the most effective way to increase hypervelocity impact resistance is to increase the thickness of the outer foil layer. Increasing the spacing between the outer surface and the substructure is also very effective at increasing dispersion.

*Research Engineers, Metals and Thermal Structures Branch, Structures and Materials Competency

Introduction

Hypervelocity impact resistance of metallic thermal protection systems (TPS) proposed for future reusable launch vehicles is an important design consideration. The impact velocity between orbiting particles (space debris and micrometeoroids) and orbiting vehicles is typically in excess of material sound speed, resulting in the term hypervelocity impact. The average relative velocity between space debris and orbiting vehicles is typically 10 km/s, but can be as high as 16 km/s. At these velocities, even small particles have sufficient momentum to significantly damage a spacecraft. Metallic TPS may cover a large percentage of the vehicle exterior surface, resulting in increased probability over the design life of the vehicle of impact with space debris and micrometeoroid particles large enough to penetrate the TPS. Penetration of the TPS may decrease the level of thermal protection provided on reentry, and the impact debris may also damage components underneath the TPS. Clearly, it is important to understand the impact resistance of metallic TPS so more impact resistant, yet efficient designs can be developed.

A review of metallic TPS development evolution is included in Reference 1. Several of the more recently developed metallic TPS concepts include a foil-gage honeycomb sandwich on the outer surface and a thin foil on the inner surface that encapsulates fibrous insulation. One such concept, a superalloy honeycomb TPS, is illustrated in Figure 1. As shown in the figure, it consists of a foil-gage honeycomb-sandwich, several inches of fibrous insulation, an inner foil backing, and the substructure. The honeycomb sandwich is made of Inconel 617 for vehicle regions that experience high temperatures during reentry and titanium for low temperature regions. The inner foil backing is made of titanium for all vehicle regions. The hypervelocity impact analysis of TPS with Inconel 617 honeycomb-sandwich and inner titanium foil is the focus of this paper.

The configuration of the metallic TPS design in the center of a panel, away from the edges and attachments, is very similar to a Whipple Shield[2], a structure used to protect satellites from space debris. As shown in Figure 2, the basic Whipple Shield design consists of one or more thin walls separated by a standoff distance from the structure being protecting. The center of a TPS

panel (excluding the fibrous insulation and honeycomb core) is similar to a Whipple Shield, consisting of three thin foil layers with spacing between them. Therefore, the TPS panel may already be in a good configuration to shield against orbital debris. But, with modification of key design parameters it may be possible to significantly enhance impact resistance. The objective of this study is to identify the most mass efficient way to improve impact resistance.

Method

In this study a computational model of a simplified configuration, representative of the center of a metallic TPS panel, was developed. Damage predicted using the model was compared to experimental results. The model was then used in a statistical sensitivity analysis to quantify and rank influences of key design parameters on impact resistance.

Model Description

Hypervelocity impact models were generated in CTH[3], a shock-physics code developed by Sandia National Laboratories. CTH can be used to solve problems involving multiple materials, large deformations and strong shocks. A finite volume technique is implemented with Eulerian mesh to solve the conservation of mass, momentum, and energy equations. Only mechanical effects are considered in this study. Electromagnetic, chemical, and heat conduction effects are neglected.

Key features of the model developed for the current study are summarized in Figure 3. An axisymmetric model was generated to reduce computational time and memory requirements, allowing workstation-class computer resources to be used. The honeycomb-sandwich-panel outer facesheet and inner facesheet will be referred to as Layer 1 and Layer 2, respectively. The honeycomb core between Layer 1 and Layer 2 was omitted. Previous computational studies show that impact normal to the outer surface at different locations relative to the core can produce significantly different responses, but that omitting the core produces an average response.[4] The Saffil fibrous insulation layer was also neglected because it could not be readily modeled with CTH. The low density insulation would attenuate the effects of the impacting particle somewhat, so that neglecting the insulation will produce a conservative result. The titanium foil layer and aluminum substructure were modeled, and will be referred to as Layer 3 and substructure, respectively.

Material modeling in hydrocodes can be broken into three categories: volumetric response, resistance to distortion, and failure.[5] Material volumetric response, or resistance to compression, is predicted using an equation-of-state (EOS). Of the three material modeling categories, volumetric response has the largest influence on hypervelocity impacts.[6] For this reason, highly detailed tabularized EOS are used with CTH that report pressure and energy as a function of density and temperature. The EOS used are valid through the range of densities and temperatures experienced in a hypervelocity impact, and account for multiple material phase changes. Material resistance to distortion, or constitutive response, is known to be in general a second order effect at the pressures involved in hypervelocity impacts.[6] This is because the impact pressure is many times in excess of material strength. For this reason, a simple elastic-plastic model with Von Mises yield surfaces was used for the hypervelocity projectile and outer TPS layers. The aluminum substructure was modeled using the more detailed Johnson-Cook viscoplastic model, since it was expected that impact pressure would be much lower in the substructure. Failure in tension was modeled using the standard CTH option in which tension is relieved by introducing a void into computational cells when the hydrostatic tensile stress exceeds fracture strength.[7]

Table 1 contains the EOS, yield strength and fracture strength values used. The SESAME[8] aluminum EOS was used for both Al 1100-O and Al 2024-T81, with a density correction factor used with Al 2024-T81 to account for the lower density due to alloying. A tabularized version of the Analytical Equation Of State (ANEOS)[9] was used for titanium foil layers. The EOS for Inconel 617 was approximated by using the EOS for nickel with a density correction factor of 1.06 to correct for the density difference.

Materials in Table 1 with a numerical entry under yield strength used an elastic-plastic model with Von Mises yield surface for material strength. The substructure was modeled using the Johnson-Cook viscoplastic model[10] with default values for 2024-T351 aluminum, since no constitutive model was available for 2024-T81. Failure in tension was modeled using the standard CTH option in which tension is relieved by introducing a void into computational cells when the mean principal stress exceeds the fracture strength. The fracture strength for 2024 aluminum is estimated from values for 2219 aluminum given by Hertel.[2] Fracture strength for titanium is derived from the dynamic flow stress reported by Babcock[11] multiplied by a factor of two, as suggested by Silling.[7] Values for the dynamic flow stress of Inconel 617 were not available. However, dynamic yield strength is typically on the order of twice the static yield strength. Fracture strength for Inconel 617 was obtained by multiplying the yield strength[12] by a factor of two (to approximate dynamic yield strength) and then multiplying by an additional factor of two (as suggested by Silling[7]).

Axisymmetric models were generated in which a rectangular mesh of computational cells was created in

a radial plane. Thus, each rectangular computational cell represents a toroid about the axis of symmetry. As shown in Figure 4, a centerline symmetric boundary condition was imposed along the axis of symmetry, preventing mass, momentum, stress deviator, and energy fluxes through the axis of symmetry. Absorbing boundary conditions were used along all other boundaries, allowing material to flow out of the computational domain. Material layers were un-restrained. Since impact occurs at velocities in excess of material sound speeds, the conditions at the edges of a material layer will not influence the response during the initial microseconds of impact, the time frame of interest.

It is standard practice to use four or more computational cells through the thickness of a layer in order to allow adequate resolution of the shock structure.[13] In addition, to insure an accurate numerical solution computational cells should be square in impacted areas and cell dimensions should only be varied gradually. A two-step Eulerian solution scheme is used in CTH which requires that both material and void be meshed. The geometry of the model in this study, with large spacing between relatively thin layers, requires an extremely dense mesh. In order to make solution of the model on the computer resources available more practical, it was decided to only require two computational cells through the wall thickness, the rationale being that the shock structure in the thin layers may not be captured completely, but that the shock structure generated in the larger, more massive incoming particle will be generated with reasonable accuracy. In a previous study, it was shown that this assumption was reasonable for problems with this geometry.[14] This reduces the required number of computational cells by a factor of 4 and total runtime by a factor of 5. Runtime is on the order of 1 CPU-day for this modeling scheme, running on an SGI MIPS R10000 CPU.

During a hypervelocity impact simulation, a large amount of low density gas is generated, which tends to dramatically increase computational run time and may lead to numerical difficulties. To avoid computational problems, a material filter was used to remove material with both density below 0.005 gm/cm^3 and pressure below 0.1 MPa. Discarding material of such low density is assumed to have a negligible effect on the simulation.

Comparison with Experimental Results

Figure 5 shows an impact simulation of an all-Titanium TPS panel, with images at several times superimposed. Impact was with a 3/16 in. particle with a 7.1 km/s velocity for correlation with experimental data reported in Reference 15. Experimental parameters are listed in Table 2. The temperatures indicated in Figure 5 are the melting point (930 K) and vaporization temperature (2300 K) of aluminum[2] at atmospheric pressure. This is to allow the state of the material to be estimated as the impact progresses. It can be seen that the outer foil layer, despite being much thinner than the projectile diameter, has shocked the projectile at 1.0 μsec, causing spalling to occur. Spalling is a tensile failure resulting from the reflection of compressive waves at free surfaces. The debris cloud is composed mostly of solid particles at this point. Upon impact with the second layer, the debris cloud is further shocked. At this time the leading edge of the debris cloud is composed of vaporous debris, with solid debris located at the center of the debris cloud. By 8.5 μsec, the debris cloud has dispersed considerably and impact is initiated with Layer 3. Predicted substructure damage from the computational models was compared to experimental data. As shown in Figure 6, agreement was very good for the titanium TPS model. The picture and computational plot are at the same scale, however the picture is a top down view of the substructure and the computational plot is a side view. The experimental hole diameter was 0.94 cm, while hole size obtained computationally was 0.78 cm. The Inconel 617 model significantly over-predicted the substructure hole size, as shown in Figure 7. The most likely explanation for the discrepancy is that the adjusted nickel EOS, used to represent Inconel 617, did not adequately represent the behavior of Inconel 617. In addition, several assumptions were required to obtain a fracture strength for Inconel 617, which may have resulted in inaccuracies. It is also possible that, in the experimental data, the particular impact location relative to the foil walls in the honeycomb core increased dispersion of the impacting particle, resulting in less substructure damage. The good correlation with experiment for the titanium honeycomb sandwich gives confidence that the modeling approach is valid. Although the lack of accurate material properties for Inconel 617 may effect the predicted damage level, it is assumed that the Inconel model would produce results that show the correct trends.

Statistical Sensitivity Analysis

The primary objective of this study is to determine the most effective place to add mass to an existing metallic TPS to improve hypervelocity impact protection. The effects of a large number of parameters or factors needed to be quantified and compared. An efficient method was needed to assess the relative importance of many factors. The conventional approach would be to investigate one factor at a time, with the remaining factors held constant. This method is acceptable for a few variables that do not change much from their baseline values. Moreover, this "one-factor-at-a-time" method assumes that the effect of each

variable is independent of variations of the other variables.

A factorial design approach can be used in which a few discrete values are chosen for each design parameter and all possible combinations are evaluated. However, the number of analyses required can quickly become unmanageable.

The method selected for this study borrows techniques commonly used in robust design.[16,17] Design parameters (independent variables) are varied simultaneously in a matrix of experiments (or in this case, analyses) defined by orthogonal arrays. The effects of a large number of design parameters, evaluated over the range of interest, can be determined efficiently using this method. The method used in this study follows closely the procedures presented in a chapter entitled "Matrix Experiments Using Orthogonal Arrays" in Reference 17 as well as similar procedures in Reference 16.

The first step in statistical sensitivity analysis is to identify the design parameters of interest. Care must be taken to select a meaningful and reasonable range of variation for each design parameter. The range of variation can affect how much each factor influences the results. The selection of the factors and their ranges usually depends on engineering experience and judgment, but a good selection is essential to formulate the problem properly for meaningful results. Several levels, usually 2 to 4, are selected to cover the range of each design parameter.

The next step in statistical sensitivity analysis is to determine what experiments or analyses need to be performed to determine the effects of the selected factors on the performance of the system. Orthogonal arrays are used to define the number of analyses to be performed and the combination of design parameter levels for each analysis. A limited number of standard orthogonal arrays[16] are available to accommodate specific numbers of design parameters with various levels per design parameters. In the orthogonal array there is a column for each design parameter, and each row is a particular combination of levels for each design parameter. The columns of the array are mutually orthogonal; that is, for any pair of columns, all combinations of design parameter levels occur, and they occur an equal number of times.[17] The smallest standard orthogonal array is chosen to accommodate the number of design parameters and design parameter levels. Any extra columns in the orthogonal array can either be ignored or in some cases used to estimate the effects of interactions between design parameters.

An experiment, or in this case an analysis, is performed for every row in the orthogonal matrix with the combination of design parameter levels defined in that row. Interpretation of the results is straightforward. The result or results for each analysis are tabulated and the overall means for all analyses are calculated. The means for each level of every design parameter are also calculated. Each column of the orthogonal matrix contains an equal number of experiments at each level of the design parameter associated with that column. The results associated with each level of that design parameter are averaged to obtain the associated means. The effect of a design parameter level is defined as the deviation it causes from the overall mean. Therefore, the effect of each design parameter level can be obtained by subtracting the overall mean from the mean associated with the particular level of that design parameter. This process of estimating the design parameter effects is sometimes called analysis of means (ANOM).

Using ANOM the effect of each design parameter, called the main effects, can be determined independently. A simple additive or superposition model is assumed for the response η:

$$\eta = overall\ mean + \sum_{\substack{design \\ parameter}} (design\ parameter\ effect) + \varepsilon \qquad (1)$$

where ε is the error of the additive approximation. Thus the response for any combination of design parameter levels can be estimated using this equation. In a typical design of experiments analysis this error term would also include a contribution associated with the error in repeatability of measuring the response, η, for a given experiment. However, for the current application the response is obtained from analysis, so error associated with measurement repeatability does not exist.

The results of ANOM can provide considerable insight into the effect of the various design parameters; however, an analysis of variance (ANOVA) can give a more accurate indication of the relative importance of the design parameters and provides a means of ranking the factors in order of importance. ANOVA can be used to determine the contribution of each design parameter to total variation from the overall mean value. The sum of squares of the differences from the mean for all the levels of a particular design parameter *(Column 5 of Table 4)* provides a measure of how much that design parameter affects the result over the specified range. The percentage that this sum of squares value contributes to the total for all design parameters ***(% Total SS** in Table 4)* gives a measure of the relative importance of that particular design parameter.

As part of the ANOVA, the error associated with the additive assumption can be estimated. The method used for the error estimate depends on the number of design parameters and design parameter levels, and the

orthogonal matrix used in the statistical sensitivity analysis.

The sum of squares due to error[17] can be calculated using the following relationship:

Sum of squares due to error =
(grand total sum of squares)
-(sum of squares due to mean) (2)
-(sum of squares due to design parameters)

where the grand total sum of squares is the sum of the squares of all values for a particular result, the sum of squares due to the mean is the overall mean squared times the number of analyses (or number of rows in the orthogonal matrix), and the sum of squares due to design parameters is the sum of squares of all the design parameter effects. There are degrees of freedom associated with each of the quantities in Equation 2. The degrees of freedom for the grand total sum of squares are the number of rows in the orthogonal matrix. There is one degree of freedom associated with the mean. Each design parameter has one less degree of freedom than the number of levels for that design parameter ***(d.o.f.** in Table 4)*. Therefore the degrees of freedom for the error can be calculated as follows:

(degrees of freedom for error) =
(number of rows in orthogonal matrix – 1) (3)
- (sum of degrees of freedom for all
design parameters)

The degrees of freedom for the error must be greater than zero for Equation 2 to be useful.

If there are zero degrees of freedom available for calculating error, as is the case in this study, a different method must be used to estimate the additive error. An approximate estimate of the sum of the squares due to error can be obtained by pooling the sum of squares corresponding to the design parameters having the lowest mean square. A rule of thumb[17] is to use the sum of squares corresponding to the bottom half of the design parameters (as defined by lower mean square) and the degrees of freedom corresponding to those design parameters. Pooled error estimates are used for the results shown in this paper.

Once the sum of square due to error and the degrees of freedom for error have been calculated, the error variance can be estimated as follows:

Error variance = (sum of squares due to error)/
(degrees of freedom for error) (4)

The variance ratio, F, is a measure of how important the effects of a design parameter are compared to the error.

F = (mean square due to a factor)/(error variance) (5)

The mean square due to a design parameter ***(Mean SS** in Table 4)* is the sum of squares of the differences from the mean for a design parameter ***(SS)*** divided by the degrees of freedom associated with that design parameter ***(dof)***.

Design Parameters

In all sensitivity analyses, a particle diameter of 3/16 in. was assumed with a normal impact velocity of 7.1 km/s. From a series of experimental impacts on metallic TPS,[15] it was found that 1/8 in. particles could be stopped by most TPS configurations without modification. All tests with larger ¼ in. diameter particles resulted in penetration of the TPS and substructure, and it was clear from the level of damage that significant modification of the TPS would be required to provide protection against a particle of this size. However, substructure damage in tests with 3/16 in. diameter particles were very sensitive to changes in TPS parameters, making this particle size interesting for study in a sensitivity analysis.

The thicknesses of each of the three layers, as well as the spacing between Layer 1 and Layer 2 and the spacing between Layer 1 and Layer 3, were selected as design parameters. Figure 8 lists the five design parameters, labeled A through E along with the design parameter levels studied. Levels were chosen that would encompass a reasonable design range for metallic TPS panels. In addition, design parameters A through C were calculated so that the difference in mass between Level 1 and Level 2 would be the same for each, 0.11 lb per panel. This is to determine the most effective location in the TPS to add mass. Level 1 and Level 2 values for design parameters D and E were chosen to encompass the design range expected for metallic TPS panels, and do not represent equal mass differences in a simple way. The change in mass for parameter D is dependent on the density of the honeycomb core. For the honeycomb used in experimental tests[18], a 0.28 in. increase in honeycomb thickness results in a 0.19 lb/ft^2 weight increase. The change in mass for parameter E is dependent on the specific metallic TPS design being used, and the method of varying the standoff between Layer 1 and Layer 3. The following discussion will focus on the metallic TPS panel design shown in Figure 1. If the insulation thickness is increased and the beaded side wall elongated to accommodate the 1 in. increase in overall TPS thickness between Level 1 and Level 2 of design parameter E, the weight increase, calculated using data from Reference 18, is 0.314 lb/ft^2. However, the increase in insulation weight accounts for 83% of this weight, and is not required. With modification, the TPS panel could be constructed with a spacer

underneath the insulation layer that would allow TPS panel thickness to be varied without increasing insulation thickness, potentially reducing the weight increase related to parameter E. There are, however, other less obvious weight penalties related to increasing the TPS panel thickness. Increasing design parameter E from Level 1 to Level 2 significantly effects the outer mold line of the vehicle, so that the impact on vehicle weight or performance may be greater than just the TPS weight increase.

Orthogonal arrays are used to define the number of analyses to be performed and the combination of design parameter levels for each analysis. A limited number of standard orthogonal arrays are available to accommodate specific numbers of design parameters with various levels per parameter.[16] An L_{16} two level orthogonal array, shown in Table 3, was selected for statistical sensitivity analysis since in this case it provides high resolution for the determination of design parameter sensitivity. The L_{16} array contains 15 columns and requires 16 experiments or analyses to be performed. Design parameters can be assigned to certain columns dependent on the orthogonal array chosen. In this study, columns 1, 2, 4, 8, and 15 were used for design parameters A through E. A signal strength, which can be thought of as a signal to noise ratio, was calculated for each column to reveal the system sensitivity to variation of the design parameters. Signals were also obtained for interactions between the design parameters. The other columns in Table 3 contain interactions between the design parameters, where "x" represents interaction. For example, AxB, located in column 3, represents the interaction between design parameters A and B. The columns containing interactions are confounded, meaning that multiple parameters are contained in the same column. In this case, each double interaction parameter is confounded with a triple interaction parameter. In the previous example, column 3 contained the interaction between design parameters C, D, and E in addition to the interaction between design parameter A and B. This indicates that predicted interaction sensitivities will be less accurate than predicted design parameter interactions. The emphasis in this research was on the effect of design parameter variation, and the design parameters were found to be more influential than the interactions. Each row represents a particular analysis, where the "1" and "2" entries in the remaining columns represent the design parameter levels. As shown in Table 3, there are 16 rows, trials 1 through 16, where each row represents a single analysis. The numbers in the row, either 1 or 2, represent the level of the design parameters for the analysis. Numbers listed in columns that only contain interactions are only used in interpretation of the results and have no influence on the design parameter levels analyzed.

Damage Metrics

Use of statistical analysis requires identification of a response, η, to be measured as a "factor of goodness", a way of quantifying the positive effect of varying design parameters. Careful selection of this factor is essential to obtaining meaningful results, and the parameter chosen should directly represent the physics involved in the process.[16]

In this study, η relates to the effectiveness of the TPS at protecting the substructure. It is a measure of the damage potential to the substructure, or in other words, a damage metric. Two forms of damage metrics were investigated: predicted substructure damage and degree of dispersion of the incoming particle.

Predicted substructure damage using hole sizes was the more intuitive damage metric, however statistical analysis using substructure hole size as a factor of goodness produced misleading results. Figure 9 shows three conceptual impact cases that reveal why this is the case. The first case, labeled "No Bumper", shows impact on an unprotected substructure, resulting in a hole approximately the size of the incoming particle. The second case, labeled "Thin Bumper", uses a Whipple Shield that results in particle break-up, but does not sufficiently disperse the particle debris cloud. The result is a substructure hole size that is larger than if the substructure was unprotected! Finally, the third case, labeled "Thick Bumper" represents an effective Whipple Shield that disperses the debris cloud to the extent that the substructure withstands the impact. If these shield designs were ranked based on substructure hole size the "No Bumper" design would be ranked above the "Thin Bumper" design, even though the thin bumper design is reducing and dispersing the impact energy.

The other form of damage metric identified focuses on the degree of dispersion of the incoming particle. In this damage metric the state of the particle debris cloud after impact with TPS, prior to substructure impact, is used. Identification of a single number that would adequately describe the degree of debris cloud dispersion was difficult. It was decided to measure what will be referred to as "Percent Momentum Radius" for several different percentage values. Percent momentum radius is defined as the radius, measured from the axis of symmetry, that contains a specified percentage of the initial projectile axial momentum. This concept is illustrated in Figure 10 for an idealized impact scenario, where 50% and 100% momentum radii are shown as a function of time. Percent momentum radius is a time dependent quantity, which requires that a consistent time be used for measurement in all of the cases examined. Because the geometry of the cases varied considerably, a fixed time was not used (for example 10 μsec.). Instead, percent

momentum radius was recorded at the initiation of substructure impact, which varied from 10 to 16 μsec after initial particle impact.

Percent momentum radius was calculated over the active computational cells only. To improve run-time and eliminate potential numerical problems, the computational cells containing Layer 1 and Layer 2 were removed after impact. In addition, momentum was lost out of the sides of the computational domain, which was sufficiently dispersed to be of no threat to the substructure but does result in a significant drop in total momentum. Due to these momentum losses, the largest percent momentum that could be used for all cases was 30%. In addition, 10% and 20% momentum radius were calculated.

Percent momentum radius was used in preference to substructure hole size beause it was more directly related to the physics of particle break-up. Use of this parameter resulted in the ranking of TPS designs based on their ability to disperse incoming particles, which had the added advantage of uncoupling the computational results from the specific substructure material and geometry simulated.

Results

TPS Design Guidelines

After completing the analyses specified in Table 3, statistical sensitivity analysis was performed for several different damage metrics. Table 4 shows representative results for the 30% momentum radius damage metric. Design parameters and interactions (these are the columns from Table 3) are listed in order of influence to the damage metric. Design parameter E has the most effect on the 30% momentum radius damage metric. Column 2 in Table 4 lists a description of the design parameters. For example, design parameter E is the spacing between Layer 1 and Layer 3. Columns 3 and 4 list the difference from mean of the damage metric at design parameter Level 1 and Level 2 respectively. In this case, design parameter E results in an average –0.17 cm decrease in the 30% momentum radius when set to 2.28 in. and a 0.17 cm increase when set to 3.28 in.. Columns 5 and 6 report the sum of squares of the damage parameter and percent total of the sum of squares. Column 7 lists the degrees of freedom of each design parameter and interaction, which is 1 in all cases because the array is limited to two levels. Column 8 is the mean sum of squares, which was calculated by dividing the sum of squares by the number of degrees of freedom.

The final step in statistical sensitivity analysis is to calculate the variance ratio, F. The variance ratio, similar to a signal to noise ratio, measures the importance of the effects of a design parameter compared to the error or noise in the results. The variance ratio, F, calculated using equation 5, is shown in column 9 of Table 4.

Table 5 lists the two most influential design parameters for each of the damage metrics examined. Statistical sensitivity analyses using 20% and 30% momentum radius both predict that a 1.0 in. variation of design parameter E will have the most influence on debris cloud dispersion. The second most influential design change was the 0.0025 in. variation of design parameter A. Both cases predict that increasing the value of these parameters will increase debris cloud dispersion and thereby provide better protection from hypervelocity impacts.

Even though it is predicted that design parameter E is more influential than design parameter A, it is likely that from a design standpoint design parameter A is the better parameter to change. Change of design parameter E, although more influential than changing A, results in a 0.314 lb increase in TPS weight, while the increase of parameter A from Level 1 to Level 2 results in a 0.11 lb increase in TPS weight. Although modifications could be made to the TPS design to reduce the weight increase associated with increasing parameter E, increasing the thickness of the TPS panel influences the outer mold line of the vehicle which will effect vehicle weight and performance. Increasing design parameter A, the thickness of Layer 1, provides additional benefits to the vehicle from an operability standpoint. Increasing the outer facesheet thickness increases the ability of the vehicle to fly through rain, resist ground hail strikes, and resist damage during assembly.

Further examination of Table 5 reveals that there is a discrepancy between predictions using 10% momentum radius as a damage metric and those using larger radii, such as 20% momentum radius and 30% momentum radius. Although there is agreement that design parameter E is influential, using the 10% momentum radius damage metric results in the prediction that a 0.28 in. variation in design parameter D is the most influential, and that the value of the parameter should be decreased to improve impact protection. This non-intuitive result led to a hypothesis that there must be some phenomena leading to the difference of predictions resulting from using 10% momentum radius as a damage metric, as opposed to the 20 or 30% momentum radius, and that the difference was probably related to the fact that 10% momentum radius measurements focus on a narrower region of the impact debris cloud than 20% and 30% momentum radius measurements. Analysis results were examined to obtain a better understanding of the phenomena leading to this discrepancy, and are discussed in the following section.

Modeling Artifacts

Examination of density and momentum data during the penetration of Layer 2 revealed a likely source for the discrepancy between the 10% damage metric, which focuses on a narrow region of the computational domain, and the 20% and 30 % damage metrics, which focus on a larger area. Momentum readings along the axis of symmetry were found to gradually decrease after impact with Layer 1, as expected, but after impact with Layer 2 momentum along the centerline increased rapidly. This is shown in Figure 11, which plots annular momentum at 0.0, 3.0, and 5.0 μsec. Annular momentum is defined in Figure 12, and is:

$$Annular\ \ Momentum(i) = \sum_{j=1}^{n} L(i, j) / A(i) \qquad (6)$$

where i and j are the radial and axial computational cell indices, L represents the axial momentum of the specified cell, and A represents the cross-sectional area of the annulus formed by the computational cell at the specified radial index. At T=0.0 μsec impact is initiated with Layer 1. At T=3.0 μsec penetration of Layer 2 is in progress, and the annular momentum has decreased substantially. However, at T=5.0 μsec, after penetration of Layer 2, a spike is seen in the annular momentum at radius of 0.0 cm, along the axis of symmetry. Examination of debris cloud radial velocity during penetration of Layer 2 revealed that as Layer 2 deforms it imparts a significant negative radial velocity to portions of the debris cloud, as shown in Figure 13. This "funnel effect" directs portions of the debris cloud to the axis of symmetry. In the axisymmetric model being used, the radial velocity of the funneled debris is set to zero when it reaches the axis of symmetry, causing debris to accumulate along the axis. The funnel effect combined with the centerline mass accumulation results in the increase of momentum along the centerline.

Estimation of the upper bound value of centerline mass accumulation revealed that from 0 to 4% of the initial axial momentum was concentrated along the centerline, depending on the configuration of Layer 1, Layer 2, and the spacing between these layers. In order to determine if this was a real phenomena or an artifact of the modeling technique a three-dimensional (3D) analysis of Layer 1 and Layer 2 was created. Results from the 3D model predicted localized funnel effects but did not predict the overall funnel effect about the centerline of the impact shown in Figure 13. Mass accumulations occurred in the 3D analysis, but were not limited to the centerline and quickly dissipated. Figure 14 shows the axial momentum distribution at T=0.0, 2.0, 4.0, and 7.0 μsec., which corresponds to the debris cloud state at the initiation of impact, after impact with Layer 1, during impact with Layer 2, and 3 μsec after impact with Layer 2, respectively. The axial momentum distribution plotted is the summation of computational cell axial momentum through y (corresponding to axial direction in axisymmetric models) at a fixed x, z location. The total momentum is then divided by the cell area in the x-z plane. As shown in Figure 14, debris cloud momentum is dispersed after impact with Layer 1. Immediately after impact with Layer 2, at T= 4.0 μsec, the axial momentum increased at several locations, which is probably due to the funnel effect. However, as shown in the axial momentum at T=7.0 μsec, the momentum increase is temporary, and the mass accumulation quickly dissipates. So, the 3D model verified that funnel effects lead to mass accumulations, however mass accumulations are not limited to the impact centerline, are not as large as in the axisymmetric model, and quickly dissipate.

The funnel effect and centerline mass accumulation explains the discrepancy between the statistical sensitivity analysis results using 10% momentum radius and larger momentum radii. Upper bound estimates of the axial momentum due to centerline mass accumulation vary from 0 to 4% of the initial axial momentum depending on the TPS configuration. Therefore, the 10% momentum radius is significantly influenced by the centerline mass accumulation, where the degree of influence will be much lower for 20% and 30% momentum radii.

Conclusion

A design of experiments approach was used with computational hypervelocity impact analyses to determine the most effective place to add mass to an existing metallic Thermal Protection System to improve hypervelocity impact protection. The choice of damage metric, used as a "factor of goodness" to rank compeating designs, was critical.

Use of percent momentum radius as a damage metric provided a good indication of the level of dispersion of the hypervelocity particle prior to impact with the substructure. Use of 20% or 30% momentum radii in sensitivity studies produced results that correspond to physical intuition. Based on these results, it is clear that the best place to add mass to increase hypervelocity impact protection is the outermost surface of the TPS panel, referred to as Layer 1. Adding mass to the outer surface not only improves hypervelocity impact protection, but increases the resistance of the panel to rain, hail, and handling damage. The spacing between the outermost layer and the substructure was also influential, and increasing this spacing will increase impact protection. However, it is likely that the penalty will be larger, both due to TPS weight directly related to the thickness of the panel, and

vehicle weight or performance that is also related to the panel thickness.

It was found that use of substructure hole size as a damage metric is potentially misleading because it is specific to an assumed substructure design and does not directly indicate the level of dispersion in the debris cloud. This may result in marginally effective protection systems being ranked lower than no protection system at all, since the marginal systems will break up the hypervelocity particle, potentially producing larger substructure holes.

The centerline mass accumulation observed in axisymmetric analysis results, termed funnel effect in this paper, is not realistic for this problem. Use of 3D models showed that the funnel effect predicted by axisymmetric models is possible, however the resulting mass accumulations are not limited to the impact centerline, were not as large, and were non-persistent. The discrepancy between 10% momentum radius sensitivity analysis results and the 20% and 30% momentum radius sensitivity results is attributed to the centerline mass accumulation. Use of 10% momentum radius as a damage metric produced unintuitive results since the focus of this measurement is the central portion of the model influenced by the centerline mass accumulation. It is concluded that 20% and 30% momentum radii measurements give a better indication of the degree of dispersion in the debris cloud.

Based on these findings, it is clear that the best place to add mass to increase hypervelocity impact protection is the outermost surface of the TPS panel.

References

[1]Blosser, M. L.: Advanced Metallic Thermal Protection Systems for Reusable Launch Vehicles. Ph.D. Dissertation, University of Virginia, May, 2000.

[2]Hertel, E. S., Jr.: Comparison of Analytic Whipple Bumper Shield Ballistic Limits with CTH Simulations. Sandia National Laboratories, SAND92-0347, Albuquerque, New Mexico, 1993.

[3]McGlaun, J. M.; et. al.: A Brief Description of the Three-Dimensional Shock Wave Physics Code CTH. Sandia National Laboratories SAND89-0607, July 1990.

[4]Poteet, C. C.: Computational Study of Hyper-velocity Impacts on Metallic Thermal Protection Systems. Presented at AIAA 8th International Space Planes and Hypersonic Systems and Technologies Conference, Norfolk, VA., April 27-30, 1998.

[5]Anderson, E., Jr.: An Overview of the Theory of Hydrocodes. Int. J. Impact Engng., Vol. 5, pp. 33-59, 1987.

[6]Hertel, E. S., Jr., Personal Communication

[7]Silling, S.: Use of the Johnson-Cook Fracture Model in CTH. Computational Physics and Mechanics Department, Sandia National Laboratories, Albuquerque, New Mexico, 1996.

[8]Kerley, G. I.: Theoretical Equations of State for Aluminum. Int. J. Impact Engng. 5, 441-449, 1987.

[9]Trucano, T. G.: Library of ANEOS Equations-of-State for CTH. Sandia National Laboratories Report, to be published.

[10]Bell, R. L.; et. al.: CTH User's Manual and Input Instructions. CTH Development Project, Sandia National Laboratories, Albuquerque, New Mexico, July, 1996.

[11]Babcock, S. G.; Kumar, A.; Green, S. J.: Final Report on Response of Materials to Suddenly Applied Stress Loads. Part I: High Strain-Rate Properties of Eleven Reentry Vehicle Materials at Elevated Temperatures. GM Defense Research Laboratories, Technical Report AFFDL-TR-67-35, Part I, April 1967.

[12]Brown, W. F., Jr.; Mindlin, H.; and Ho, C. Y.: Aerospace Structural Metals Handbook, CINDA/USAF CRDA Handbooks Operation, Purdue Univ., 1994.

[13]Hertel, E. S., Jr.; Chhabildas, L. C.; Hill, S. A.: Whipple Bumper Shield Simulations. Shock Compression of Condensed Matter 1991, S. C. Schmidt, R. D. Dick, J. W. Forbes, D. G. Tasker (editors), Elsevier Science Publishers, New York, 1992.

[14]Poteet, C. C.: Computational Study of Hypervelocity Impacts on Metallic Thermal Protection Systems. Masters Thesis, The George Washington University, August, 1998.

[15]Karr, K. L.; Poteet, C. C.; Blosser, M. L.: Hypervelocity Impact Test Results for a Metallic Thermal Protection System. NASA TM, publication pending.

[16]Ross, P. J.: Taguchi Techniques for Quality Engineering: Loss Function, Orthogonal Experiments, Parameter and Tolerance Design, Second edition, McGraw-Hill, New York, 1996.

[17]Phadke, M. S.: Quality Engineering using Robust Design, Prentice Hall, Englewood Cliffs, NJ, 1989.

[18]Myers, D. E.; Martin, C. J.; Blosser, M. L.: Parametric Weight Comparison of Advanced Metallic, Ceramic Tile, and Ceramic Blanket Thermal Protection Systems. NASA TM-2000-210289, Langley Research Center, Hampton, VA, June, 2000.

Table 1: CTH Material Parameters

Material	Equation of State	Yield Strength (MPa)	Fracture Strength (MPa)
1100-O Al	SESAME Aluminum	34	-100
2024-T81 Al	SESAME Aluminum	Johnson-Cook	-1500
Ti 6-4	ANEOS Ti 6-4	880	-2860
Inconel 617	ANEOS Ni	350	-1400

Table 2: Experimental Parameters

Experiment Parameters	Inconel TPS	Titanium TPS
Outer Facesheet		
Material	INC 617	Ti-6AL-4V
Gauge (in)	0.005	0.005
Honeycomb Core		
Material	INC 617	Ti-6AL-4V
Cell Size (in)	0.25	0.1875
Gauge (in)	0.002	0.0015
Depth (in)	0.28	0.28
Inner Facesheet		
Material	INC 617	Ti-6AL-4V
Gauge (in)	0.005	0.005
Insulation		
Material	Saffil	Saffil
Thickness (in)	2.0	2.0
Density (lb/ft^3)	1.5	1.5
Titanium Foil		
Material	Ti-6AL-4V	Ti-6AL-4V
Gauge (in)	0.003	0.003
Substructure		
Material	2024-T81 Al	2024-T81 Al
Thickness (in)	0.1	0.1

Table 3: L16 Two-Level Orthogonal Array. Design parameters located on columns 1, 2, 4, 8, 15. Two way and three way interactions located on remaining columns.

	Column Number														
	1	2	3	4	5	6	7	8	9	10	11	12	13	14	15
Trial #	A	B	AxB, CxDxE	C	AxC, BxDxE	BxC, AxDxE	DxE, AxBxC	D	AxD, BxCxE	BxD, AxCxE	CxE, AxBxD	CxD, AxBxE	BxE, AxCxD	AxE, BxCxD	E
1	1	1	1	1	1	1	1	1	1	1	1	1	1	1	1
2	1	1	1	1	1	1	1	2	2	2	2	2	2	2	2
3	1	1	1	2	2	2	2	1	1	1	1	2	2	2	2
4	1	1	1	2	2	2	2	2	2	2	2	1	1	1	1
5	1	2	2	1	1	2	2	1	1	2	2	1	1	2	2
6	1	2	2	1	1	2	2	2	2	1	1	2	2	1	1
7	1	2	2	2	2	1	1	1	1	2	2	2	2	1	1
8	1	2	2	2	2	1	1	2	2	1	1	1	1	2	2
9	2	1	2	1	2	1	2	1	2	1	2	1	2	1	2
10	2	1	2	1	2	1	2	2	1	2	1	2	1	2	1
11	2	1	2	2	1	2	1	1	2	1	2	2	1	2	1
12	2	1	2	2	1	2	1	2	1	2	1	1	2	1	2
13	2	2	1	1	2	2	1	1	2	2	1	1	2	2	1
14	2	2	1	1	2	2	1	2	1	1	2	2	1	1	2
15	2	2	1	2	1	1	2	1	2	2	1	2	1	1	2
16	2	2	1	2	1	1	2	2	1	1	2	1	2	2	1

Table 4: Analysis of Variance for 30% Momentum Radius Damage Metric

30% Momentum Radius		Difference from Mean, cm		Sum of	% Total	d.o.f.	Mean	F
Factor		Level 1	Level 2	Squares	SS		SS	
E	Spacing Layer 1 / Layer 3	-1.74E-01	1.74E-01	4.87E-01	46.49	1	4.87E-01	46.06
A	Thickness Layer 1	-1.13E-01	1.13E-01	2.05E-01	19.56	1	2.05E-01	19.39
D x E	Interaction	8.19E-02	-8.19E-02	1.07E-01	10.25	1	1.07E-01	10.15
A x D	Interaction	6.31E-02	-6.31E-02	6.38E-02	6.09	1	6.38E-02	6.04
D	Spacing Layer 1 / Layer 2	-4.94E-02	4.94E-02	3.90E-02	3.73	1	3.90E-02	3.69
C x D	Interaction	4.94E-02	-4.94E-02	3.90E-02	3.73	1	3.90E-02	3.69
B	Thickness Layer 2	-3.69E-02	3.69E-02	2.18E-02	2.08	1	2.18E-02	2.06
*A x E	Interaction	3.56E-02	-3.56E-02	2.03E-02	1.94	1	2.03E-02	
*C	Thickness Layer 3	-3.19E-02	3.19E-02	1.63E-02	1.55	1	1.63E-02	
*B x C	Interaction	-3.06E-02	3.06E-02	1.50E-02	1.43	1	1.50E-02	
*A x B	Interaction	-2.94E-02	2.94E-02	1.38E-02	1.32	1	1.38E-02	
*C x E	Interaction	2.69E-02	-2.69E-02	1.16E-02	1.10	1	1.16E-02	
*B x D	Interaction	1.69E-02	-1.69E-02	4.56E-03	0.44	1	4.56E-03	
*B x E	Interaction	1.19E-02	-1.19E-02	2.26E-03	0.22	1	2.26E-03	
*A x C	Interaction	-6.87E-03	6.87E-03	7.56E-04	0.07	1	7.56E-04	
Pooled Error (*)				(8.E-02)		(8)	(1.E-02)	
			Total	1.05E+00	100.00			

Table 5: Recommended change in design parameters determined using different damage metrics

Rank	10% Momentum Radius	20% Momentum Radius	30% Momentum Radius
1	Decrease D	Increase E	Increase E
2	Increase E	Increase A	Increase A

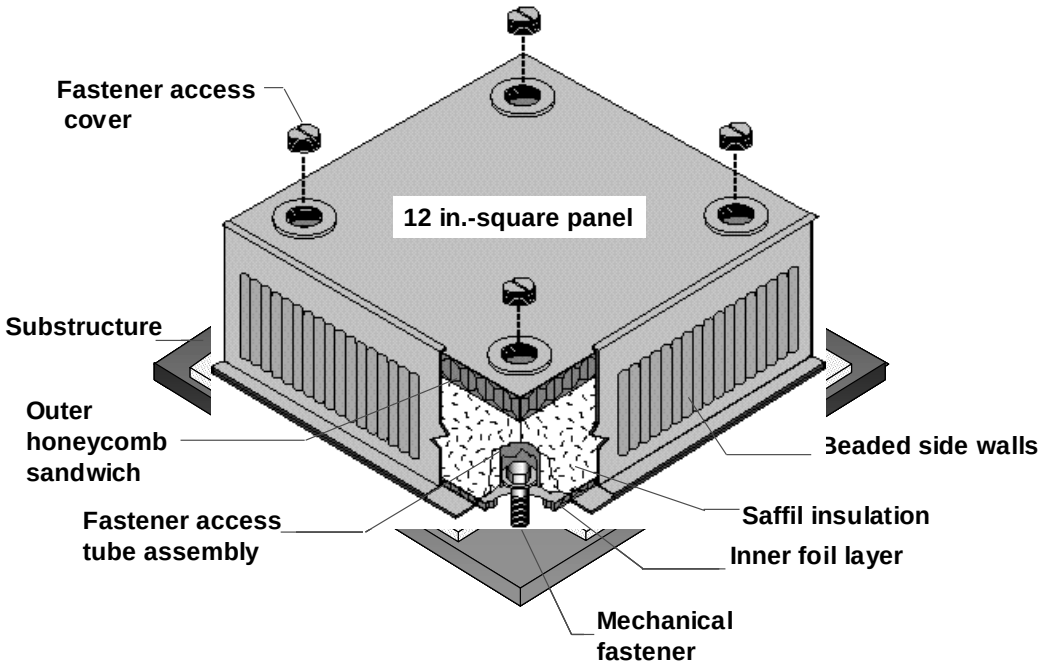

Figure 1: Metallic TPS Panel

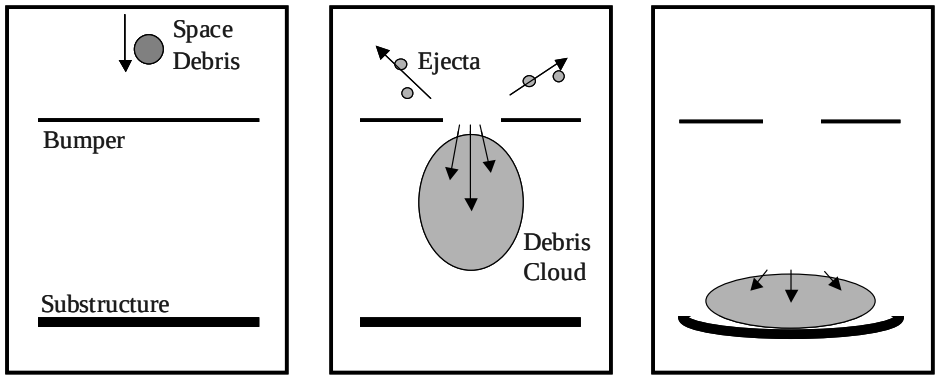

Figure 2: Basic Whipple Shield design principle

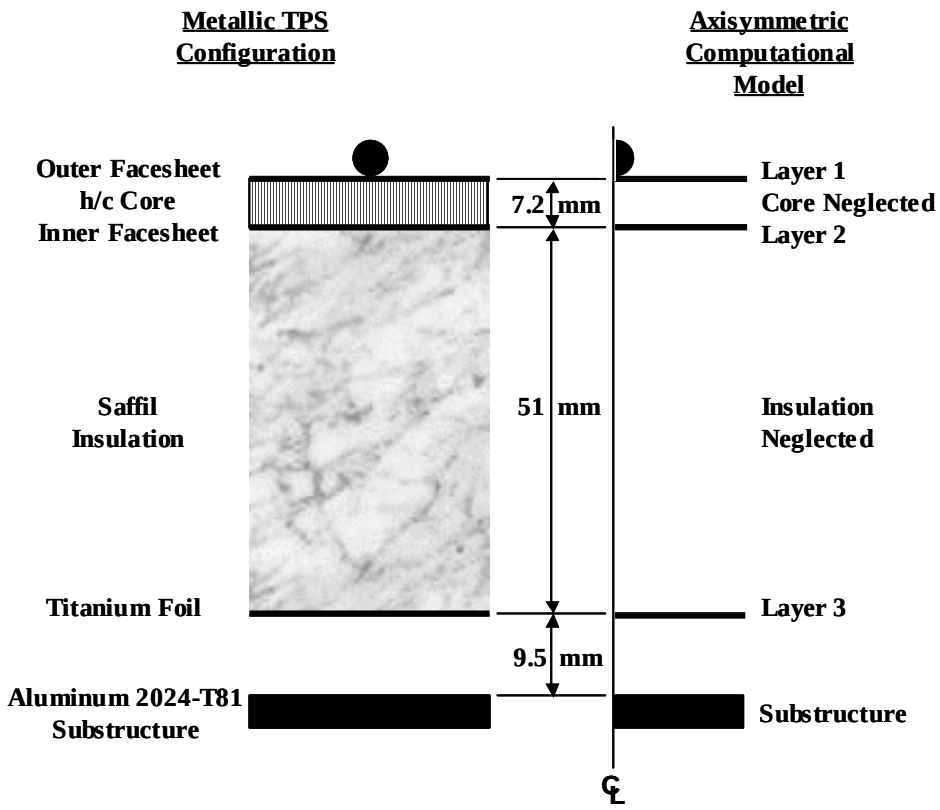

Figure 3: Comparison of Experimental Configuration (through the thickness) to Axisymmetric Computational Model

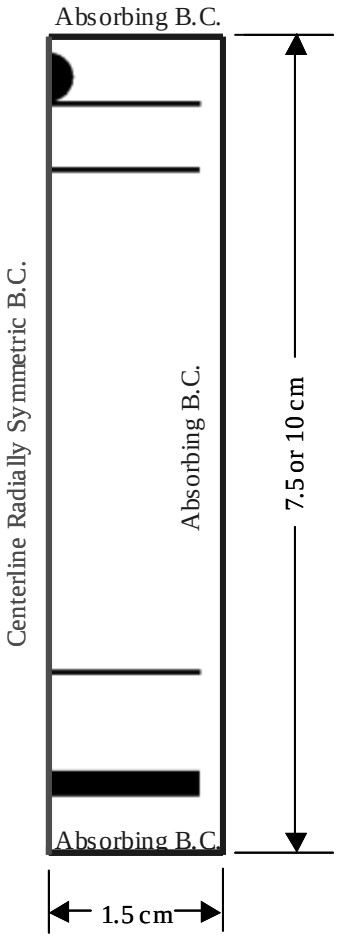

Figure 4: Schematic representation of axisymmetric finite volume model created for use with CTH.

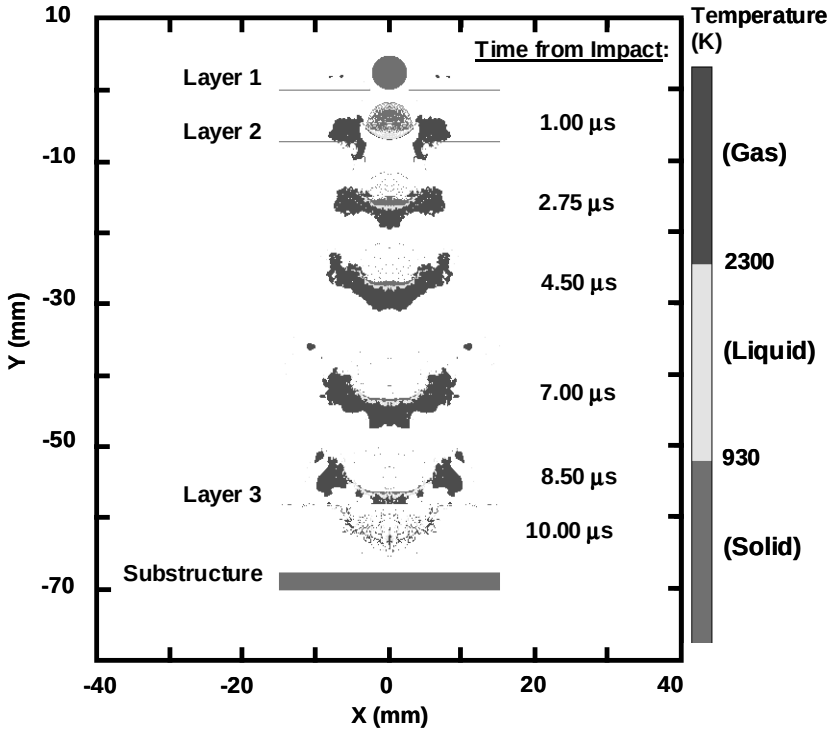

Figure 5: Time elapsed view of computational simulation of hypervelocity impact on titanium TPS

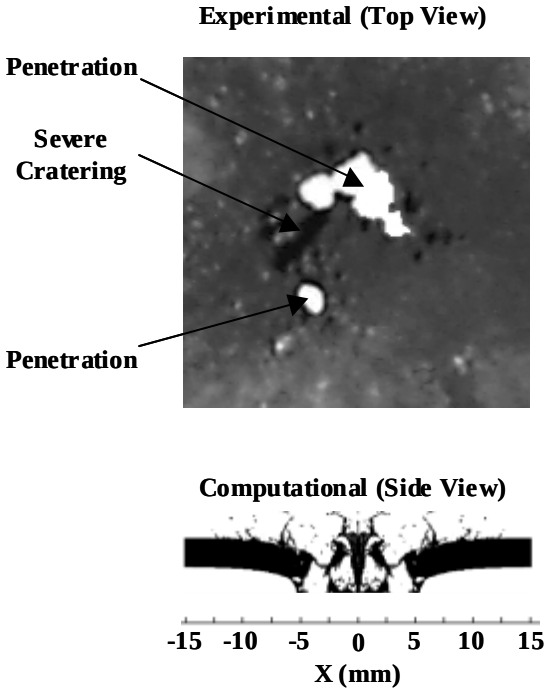

Figure 6: Comparison of Predicted and Measured Substructure Damage for Titanium TPS

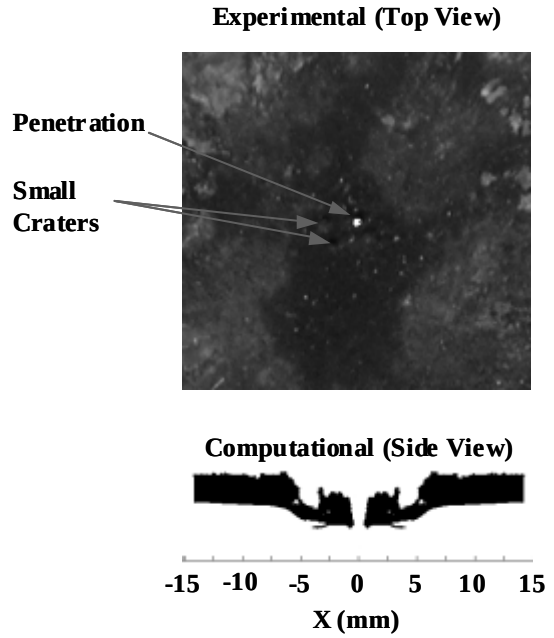

Figure 7: Comparison of predicted and measured substructure damage for Inconel TPS

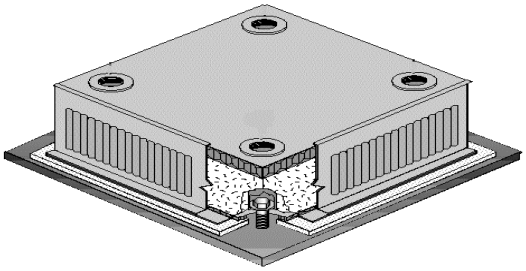

Metallic TPS Design

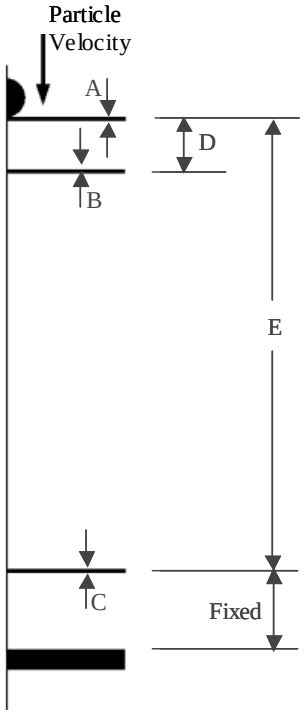

Axisymmetric Model of Metallic TPS

Parameter Levels Studied

Design Parameter	Level 1 (in)	Level 2 (in)	Description
A	0.005	0.0075	Thickness Layer 1
B	0.005	0.0075	Thickness Layer 2
C	0.003	0.0077	Thickness Layer 3
D	0.28	0.56	Spacing 1
E	2.28	3.28	Spacing 2

Figure 8: Definition of parameter levels used in sensitivity analysis

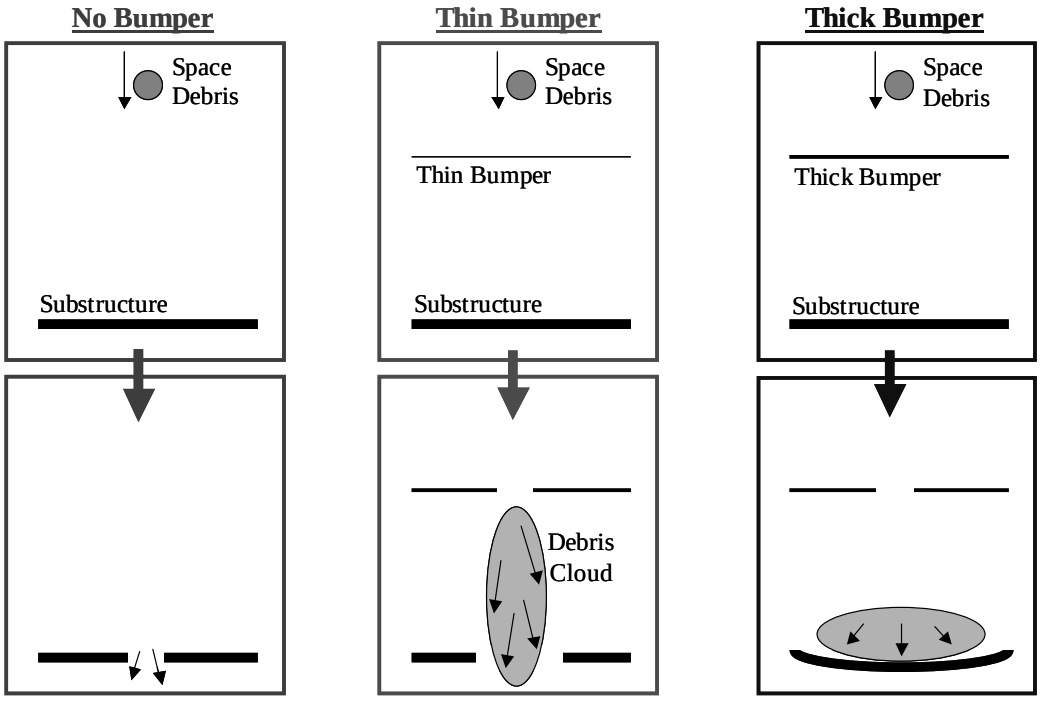

Figure 9: Schematic representation of hypervelocity impact with three different shielding configurations.

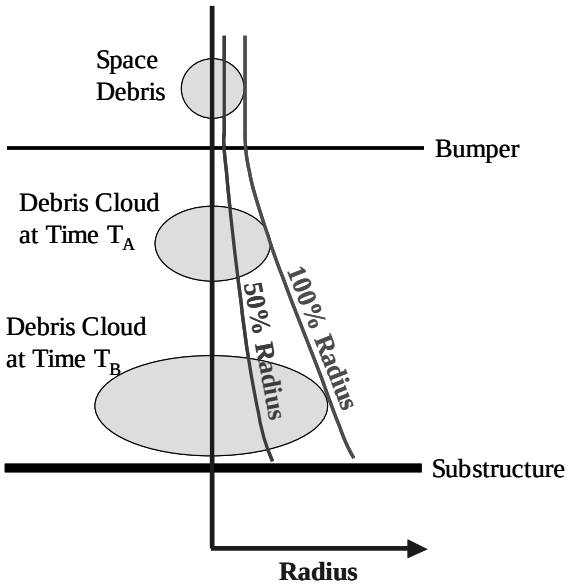

Figure 10: Explanation of percent momentum radius using idealized diagram of axisymmetric impact problem, with debris cloud shown at several arbitrary times.

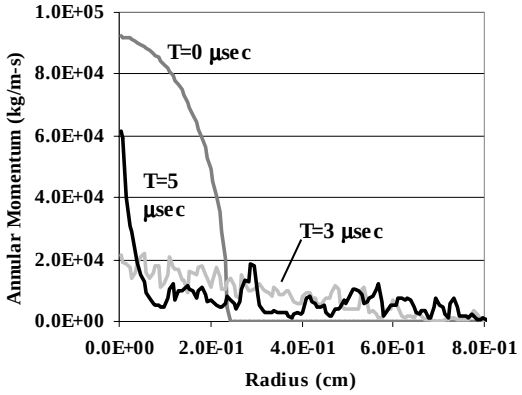

Figure 11: Annular momentum distribution in typical axisymmetric simulation, revealing centerline mass accumulation after impact with Layer 2 (at 5 μsec.)

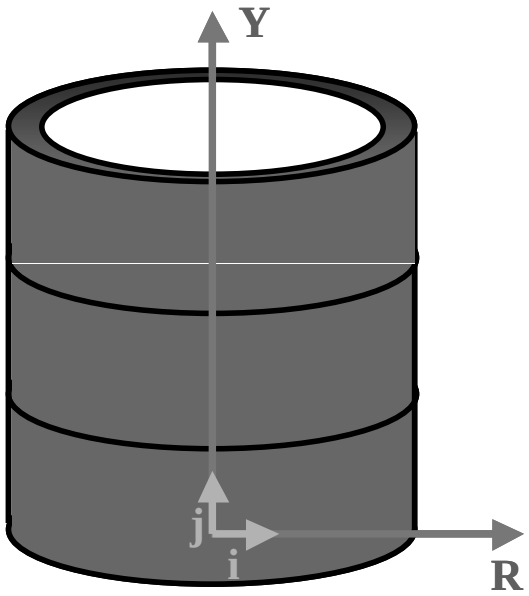

$$Annular\,Momentum(i) = \sum_{j=1}^{n} L(i, j) / A(i)$$

Figure 12: Schematic showing the summation of axial momentum in annular elements, where L(i, j) represents the axial momentum of annular element at radial indice i and axial indice j.

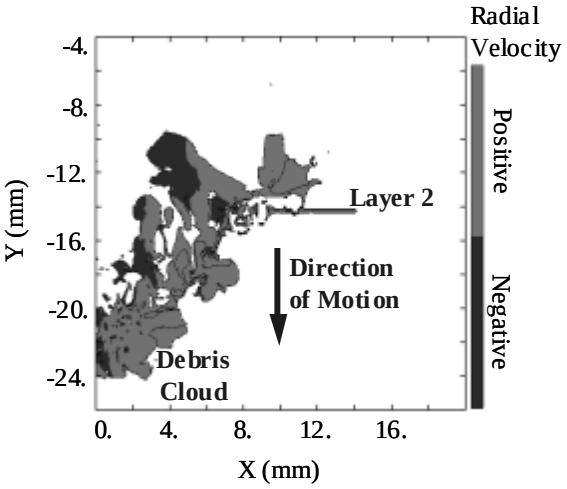

Figure 13: Initiation of funnel effect during penetration of Layer 2

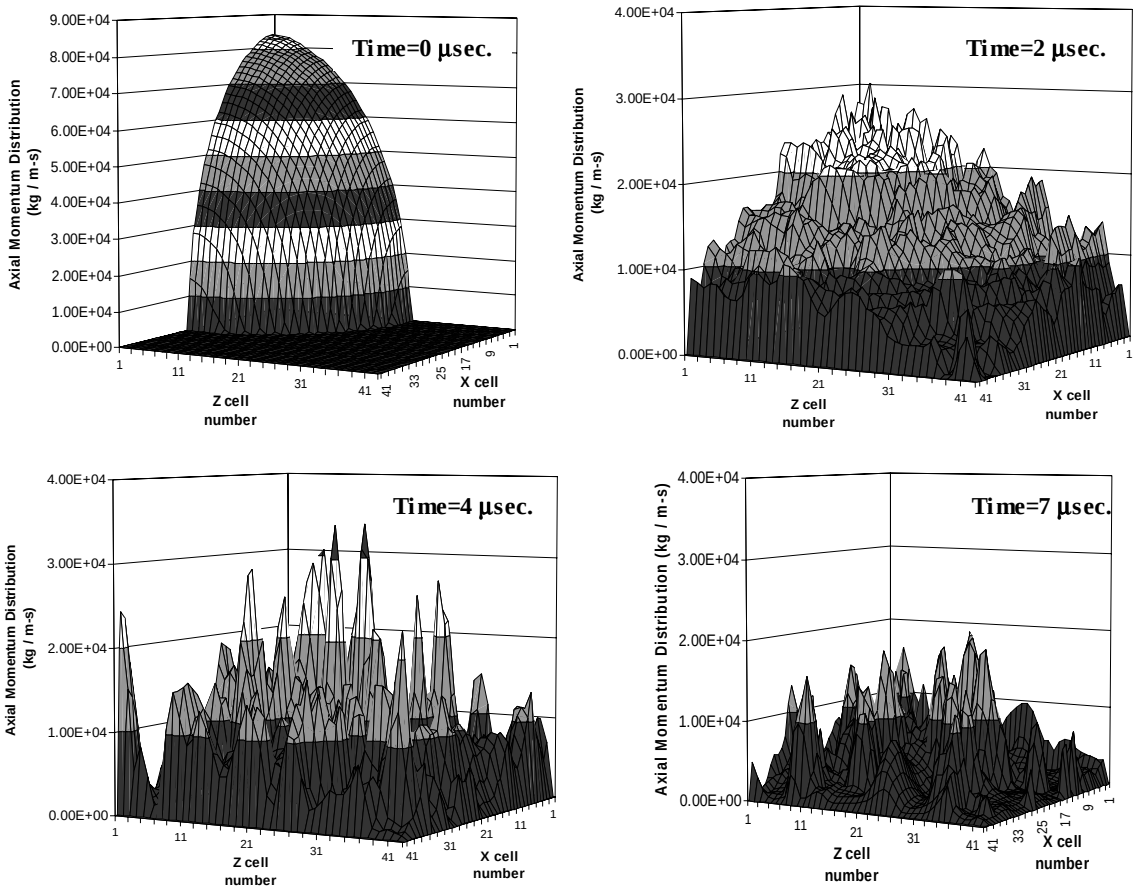

Figure 14: Axial momentum distribution at four timesteps for three-dimensional model. Momentum spikes at 4. µsec. reveal possible funnel effects. However, funnel effects are non-persistent and do not lead to centerline mass accumulation as predicted in axisymmetric model.